ORIGINAL PAPER

Application of remote sensing techniques to identify iron ore deposits in the Central Eastern Desert, Egypt: a case study at Wadi Karim and Gabal El-Hadid areas

Sobhi Mahmoud Ghoneim[1] · Salem Mohamed Salem[1] · Kareem Hamed Abd El-Wahid[1] · Mohamed Anwar[1] · Mahmoud Abd El-Rahman Hegab[1] · Nehal Mohamed Soliman[1] · Hala Fouad Ali[1]

Abstract

The integration of remote sensing, spectral measurements and field verification helped in discriminating new iron occurrences hosted in the metavolcanic rocks at Wadi Karim and Gabal El-Hadid areas in the Central Eastern Desert (CED) of Egypt. The iron host rocks were carefully recognized through different image processing techniques that were applied on Landsat-8 satellite image data with the implementation of the spectral signatures of the various iron minerals and host rocks. The detected iron ore is found in the form of Banded Iron Formation (BIF), veins and lenses of varied thicknesses ranging from a few centimetres to 5 m. They are composed mainly of magnetite and hematite, as well as accessories of aluminium, iron silicates and quartz. Moreover, the structure controls on iron ore occurrences were also illustrated in the investigated areas. The alignment of the iron forms with the primary and secondary structural planes of their host rocks may indicate the origin and mode of occurrence of the explored iron ore, as contemporaneous and syngenetic deposition with the solidification of the host metavolcanics. Several remote sensing techniques including Crosta principal component analysis (CPCA), constrained energy minimization (CEM) supervised classification technique and a newly proposed Landsat-8 band ratio (band6/band2) were applied for discriminating the iron-rich localities within the studied areas. These techniques showed high efficiency and applicability in the accurate delineation of the iron-enriched areas; this was validated through the field study.

Keywords Remote sensing · Iron exploration · Wadi Karim · Gabal El-Hadid · Egypt

Introduction

This study focuses on iron exploration at Wadi Karim and Gabal El-Hadid areas in the Central Eastern Desert (CED) of Egypt, where the existing several iron occurrences (e.g. Wadi Karim, Wadi El-Dabbah, Um Shadad, Um Ghamis El Zarga, Um Nar and Gabal El-Hadid) (e.g. Hussein 1990; El-Shazly and Khalil 2014) are considered as guide and motivation to explore new iron rich occurrences in the similar exposed rock units in these areas. The geological environments of such areas were analysed and investigated for indicating the potential iron localities.

✉ Mahmoud Abd El-Rahman Hegab
  mah_hegab94@hotmail.com

1 The National Authority for Remote Sensing and Space Sciences (NARSS), Cairo, Egypt

Gross (1980) distinguished two types of Archean–Paleoproterozoic BIF: (1) Algoma type of exhalative volcano-sedimentary origin that happened during the Late Archean (Pufahl 2010) and (2) superior type of continent-derived origin mostly of Paleoproterozoic age (Trendall and Blockley 2004). Several BIF occurrences of Neoproterozoic age have been discussed e.g. Rapitan from Canada (Klein and Beukes 1993), Damara from Namibia (Breitkopf 1988), Urucum from Brazil (Klein and Ladeira 2004), Adelaide Geosyncline from South Australia (Lottermoser and Ashley 2000), Menhouhou from Morocco (Pelleter et al. 2007) and BIF from the Arabian–Nubian Shield of Egypt and Saudi Arabia (El Habaak 2005; El-Shazly and Khalil 2014). James et al. (1992) defined four BIF mineral assemblages, namely, oxide facies including magnetite and hematite subfacies, silicate facies, carbonate facies and sulphide facies. BIFs are considered as products of diagenetic and metamorphic alteration of Fe-rich, chemically precipitated marine sediments with a minimum of 15% Fe (Klein and Beukes 1993; Mücke

et al. 1996). Moreover, various models were proposed for the source of Fe and Si. Holland (1973) assumed hydrothermal leaching of submarine basalt. Garrels (1987) mentioned surface weathering of continents. Krapez et al. (2003) proposed volcanogenic supplies. Pickard et al. (2003) assumed that the sources of Fe and Si are the palaeo-environment of deposition and the paragenetic sequence of the iron oxides. The most accepted model indicates that Fe and Si were mainly leached by seawater circulation at mid-ocean ridges and transported in a largely anoxic ocean on the continental shelf where upwelling and/or photosynthesis caused the oxidation of Fe^{+2} and its precipitation as oxide bands (Lascelles 2013).

Remote sensing data have been widely used for alteration mapping and mineral exploration (e.g. Ghoneim, et al. 2021, 2022; Moradpour, et al. 2020, 2022; and Sekandari, et al. 2022). Also, remote sensing data were used to locate areas of iron oxides and/or hydrous minerals in arid and semi-arid environments (Abrams et al. 1983; Kaufman and Sendra 1988; Bhattacharya, et al. 1993, Ammar, et al. 1993, Aiken, et al. 1997, Tangestani and Moore 2001; Ramadan and Kontny 2004; Salem et al. 2013; Salem and Gammal 2015; Duuring and Laukamp 2016; Mao et al. 2019; Traore et al. 2020; Gopinathan et al. 2020 and Guha et al. 2020). Moreover, Sabins (1997) suggested an ETM + band ratio 3/1 to discriminate iron-rich rocks from all other rock units. The band ratios 3/1 in ETM + and 4/2 in Landsat-8 are more effective in iron exploration because iron minerals have significant reflectance and absorption in these bands. Band ratio technique enhances spectral differences and reduces the effect of topography so enabling more precise discrimination (Sabins 1997). Ciampalini et al. (2013) used remote sensing techniques for exploration of iron deposits in the Western Sahara and southwest of Algeria. Salem et al. (2013) studied the west Lake Naser area using ETM + images and suggested three areas of iron ore potentiality at Kurkur, Abu Simbil and Tushka areas. This study aims at exploring and locating new iron occurrences at Wadi Karim and Gabal El-Hadid areas, where the known iron occurrences and their specific environments were used as remarks and guides for exploring other similar environments of potential iron ore occurrence.

The study areas

The study areas lie in the CED of Egypt between latitudes from 25° 53′ to 26° 00′N and longitudes from 34° 00′ to 34° 10′ E for Wadi Karim area and latitudes from 25° 20′ to 25° 24′ N and longitudes from 34° 07′–34° 11′ E for Gabal El-Hadid area (Fig. 1). Both the study areas are highly accessible through desert routs within the Wadis dissecting these areas. Wadi Karim area lies south Quseir-Qift highway; it is accessible through a route located 15 km west of Quseir city.

Gabal El-Hadid area is accessible through Wadi Um Gheig and Wadi Mubarak through desert routes as well.

Geological setting

The study area is a part of the Pan-African belt of the Arabian-Nubian Shield (ANS). It is built up of gneisses, migmatites, metasediments, ophiolitic rocks, calc-alkaline metavolcanics, mafic intrusions, tonalite, granodiorite, Dokhan volcanics, Hammamat molasse sediments, post tectonic granites, trachytes and felsites (Fig. 2). The ophiolitic rocks are thrusted over the metavolcanics whereas some mineralized alteration zones rich in sulphides, iron oxides and talc carbonates are observed. The island arc assemblages are intruded by later phase of mafic intrusions of younger pyroxene gabbros. As well as next stage of acidic intrusions of tonalite, granodiorite and alkali feldspar granites associated with mineral bearing hydrothermal solutions, forming halos of alterations in the surrounding rocks. Several mafic and felsic dykes are dissecting the basement rocks, which are found — in some areas — unconformably overlain by Phanerozoic Cretaceous and Miocene sedimentary rocks (EGSMA 1997).

Structurally, the study areas were subjected to normal, wrench and thrust faults in addition to strike-slip shear zones. The normal faults are the older and were formed at different phases. The microlinears are conforming to the major structures. In the country rocks, primary structures such as banding, layering and bedding are present. In the Dokhan volcanics and Hammamat sediments, some primary features can be observed because of the weak deformation in these rocks (Loizenbauer et al. 2001; Abd El-Wahed et al. 2016; Hamimi and Abd El-Wahed 2020).

Data used in the study

Several datasets were implemented in the present study including (1) geological maps of the case study areas (after EGSMA 1997), (2) Landsat-8 satellite data covering the study area (Scene ID: LC81740422021031LGN00, acquired on 31/01/2021), (3) spectral signatures of iron minerals from the USGS spectral library ENVI v. 5.3) and (4) field data.

Methodology

In this study, the integrated remotely sensed data and the measured spectral characteristics of the rock varieties verified by field work have been interpreted for differentiating the iron-rich rocks as an approach for iron exploration (Fig. 3).
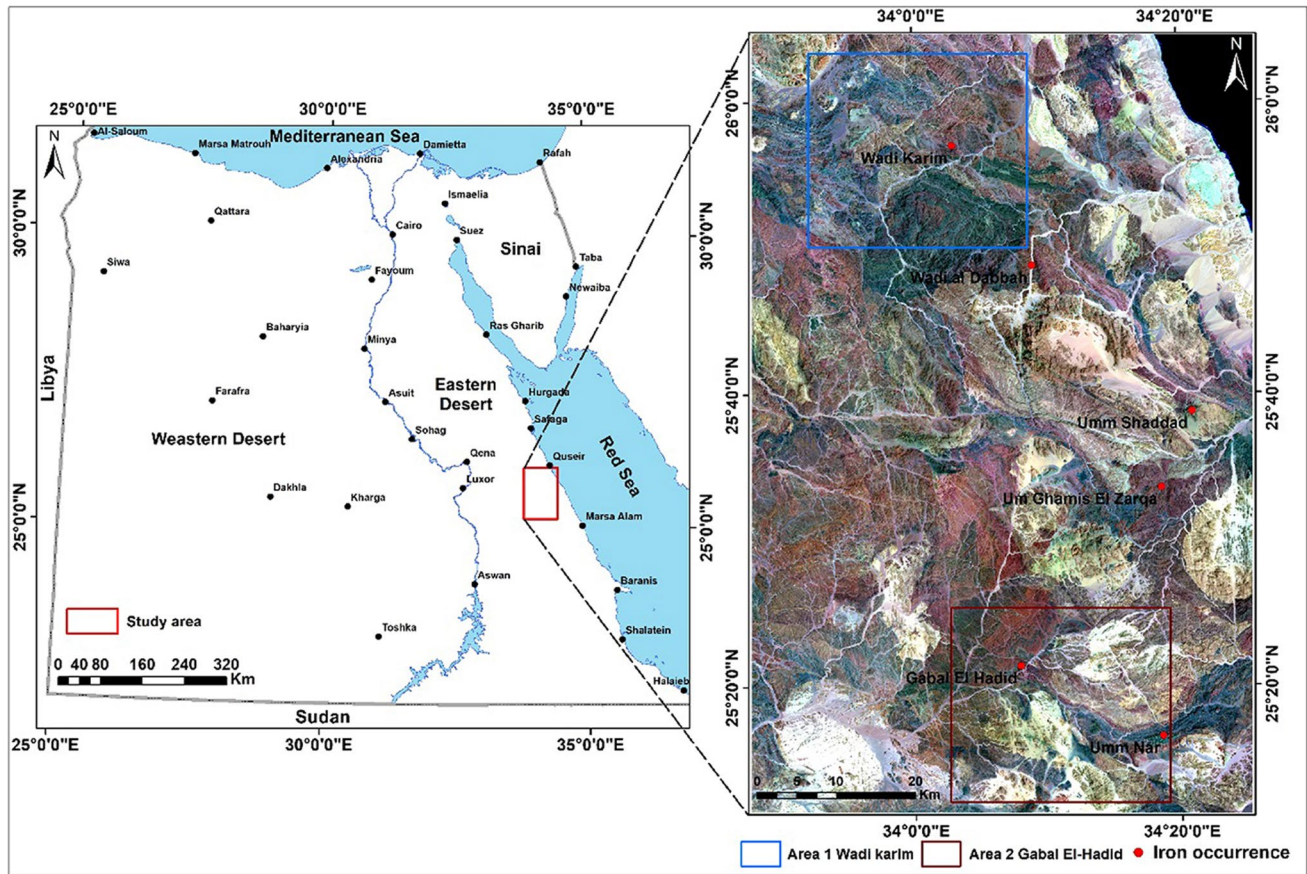
Fig. 1 Left hand image; base map of Egypt. Right hand image; Landsat-8 false colour composite of 7, 5 and 3 in RGB showing the locations of the investigated areas; Wadi Karim area in blue boundary, and Gabal El-Hadid area in brown boundary

Remote sensing

Various image processing techniques were applied — using the ENVI v. 5.3 image processing software — on Landsat-8 satellite image data to highlight the lithology and to differentiate the iron occurrences and their spatial distribution over the studied areas. The used techniques include "Crosta principal component analysis" (CPCA) technique, "band ratio" (BR) technique and the signature-based Supervised Classification techniques named "constrained energy minimization" (CEM) technique.

CPCA

Principal component analysis (PCA) is a linear transformation of axes of the original data to produce uncorrelated spectral bands. This allows removing the redundancy and noise in the data and leaving only the data with maximum variance and least correlation.

Crosta method (Crosta et al. 2003) comprises examination of the eigenvectors to identify the contributions from original bands (− ve or + ve) to each PC to select specific PCs for displaying and concentrate the desired spectral features by highlighting them as bright or dark pixels based on their respective eigenvector values magnitudes and signs (− ve eigenvector value indicates absorption while + ve ones mean reflectance). This technique was used for mineral exploration on bands of Landsat TM data (Crosta and Moore 1989; Loughlin 1991; Ruiz-Armenta and Prol-Ledesma 1998; Tangestani and Moore 2002; Carranza and Hale 2002) and on ASTER data (Moradpour, et al. 2022; and Sekandari et al. 2022). Crosta and Moore (1989) studied the spectral signatures of the alteration minerals from the US Geological Survey (USGS) spectral library, from the analysis of the spectral behaviour of these alteration minerals; they defined the best four bands for each alteration mineral: two representing the maximum reflectance and the other two representing the absorption features. Similar to the Corsta approach; the spectral behaviour of the main four iron minerals (hematite, goethite, magnetite and limonite) was investigated. The bands of maximum and minimum reflectance were defined; they were found to be bands (4 and 6) for maximum reflectance and bands (2 and 5) for absorption.
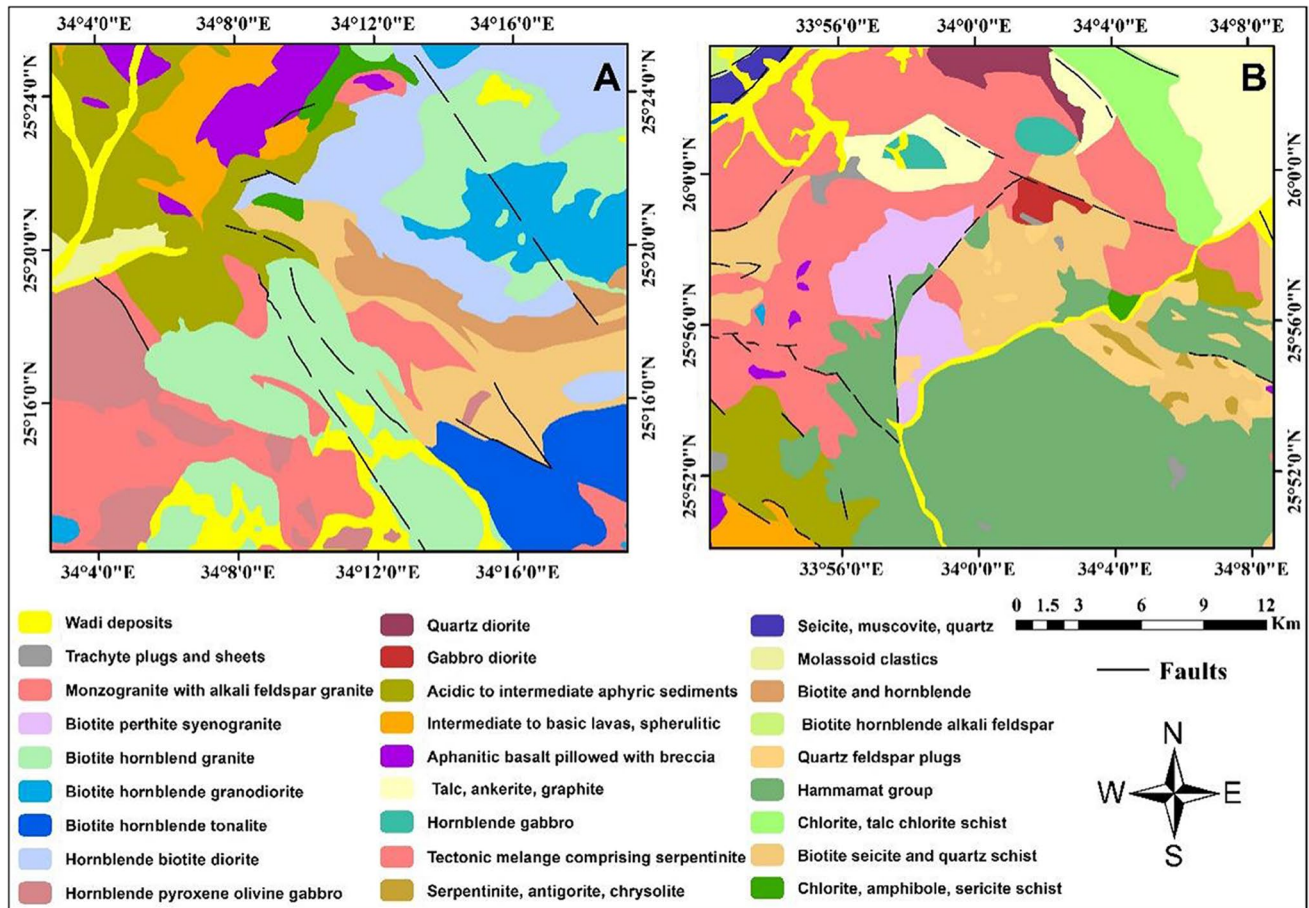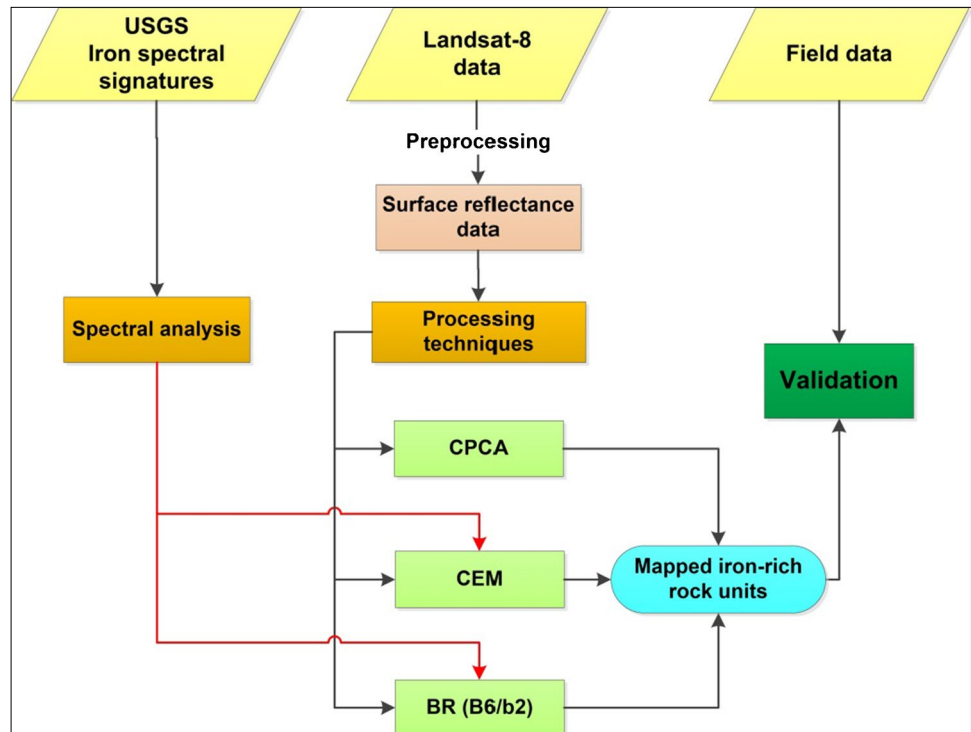
Fig. 2 Geological map of **A** Gabal El-Hadid and **B** Wadi Karim study areas (after EGSMA 1997)

Fig. 3 Methodology flow chart of the study

BR technique

Band rationing is an effective method for distinguishing among mineral/rock types because the main differences in visible, near-infrared and shortwave-infrared spectral regions are found along the slopes of the reflectivity curves. Ratio images are obtained by dividing the digital number, radiance or reflectance in one band by the corresponding value in another band for each pixel, and then the resulting values are stretched plotted as new —ratio— image (Sabins1997). For iron mapping, there are common Landsat-8 ratios that are most widely used, such as (b4/b2) which were effectively used to differentiate the iron oxides and hydroxide-rich rocks (Ducart et al. 2016 and Sadiya et al. 2014). In the present study, the Landsat-8 band ratio of b6/b2 is proposed to map the different iron minerals. This ratio is proposed based on the spectral analysis of the signatures of various iron minerals (hematite, goethite and limonite), where the highest reflectance is found associated with band (6) and the lowest reflectance is associated with band (2) (Fig. 4). The ratio of b6/b2 is found effective in discriminating the iron minerals in the study area.

CEM

The spectral reflectance of the various iron minerals was extracted from the ENVI USGS spectral library and was used as the input for the CEM-supervised classification technique. CEM technique maximizes the target spectrum response and suppresses the response of all the other features considering them as unknown background. As a result of this technique, fraction grey scale images were obtained; density slicing was performed on these images to delineate the most concentrated iron rich areas. All the delineated areas were then grouped together and considered as iron-rich units.

Field geology, sampling and measurements

Geological field studies have been conducted to the study area for field verification of the remote sensing results. The country rocks and the hosted iron deposits, as well as the newly detected iron localities, have been studied and sampled at Wadi Karim and Gabal El-Hadid areas (Fig. 5a and b). Field measurements of the different observed iron rich units were made using the hand-held "TerraSpec. Halo mineral identifier".

Results

### Interpretation of the processed satellite images

a. CPCA

   Through the analysis of the spectral signatures of the iron minerals, it is found that these minerals have remarkable high reflectance values corresponding to bands 4 and 6 besides low reflectance in bands 2 and 5 in the VNIR-SWIR spectral region of Landsat-8 data; these four bands were used as input bands in PCA transformation process producing four principal component bands (PCs) with their eigenvector statistics shown in Tables 1 and 2 for Wadi Karim and Gabal El-Hadid areas of study, respectively.

   Following the Crosta technique procedures, careful inspection of the eigenvector matrixes of the principal

Fig. 4 The spectral curves of the iron minerals from the USGS spectral library resampled to match the Landsat-8 bands
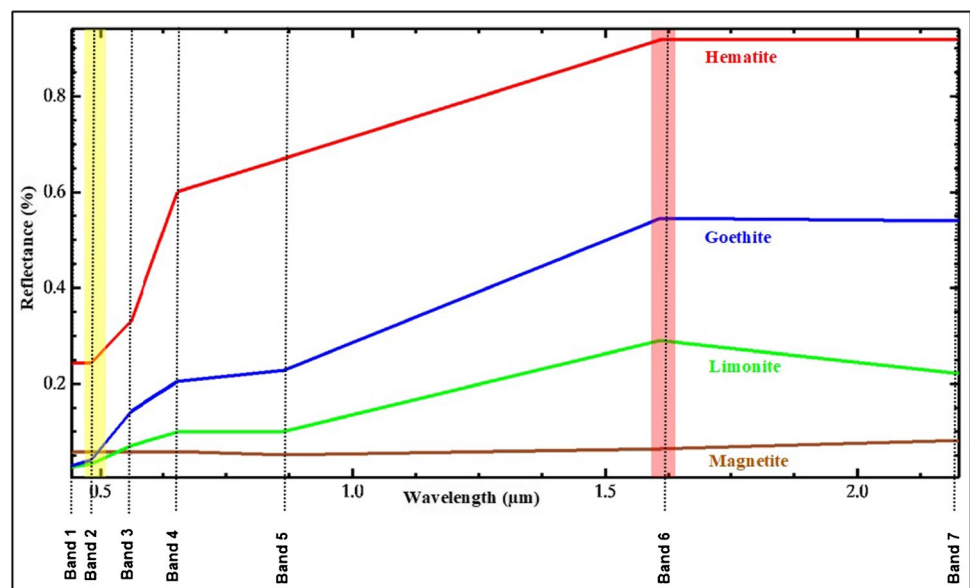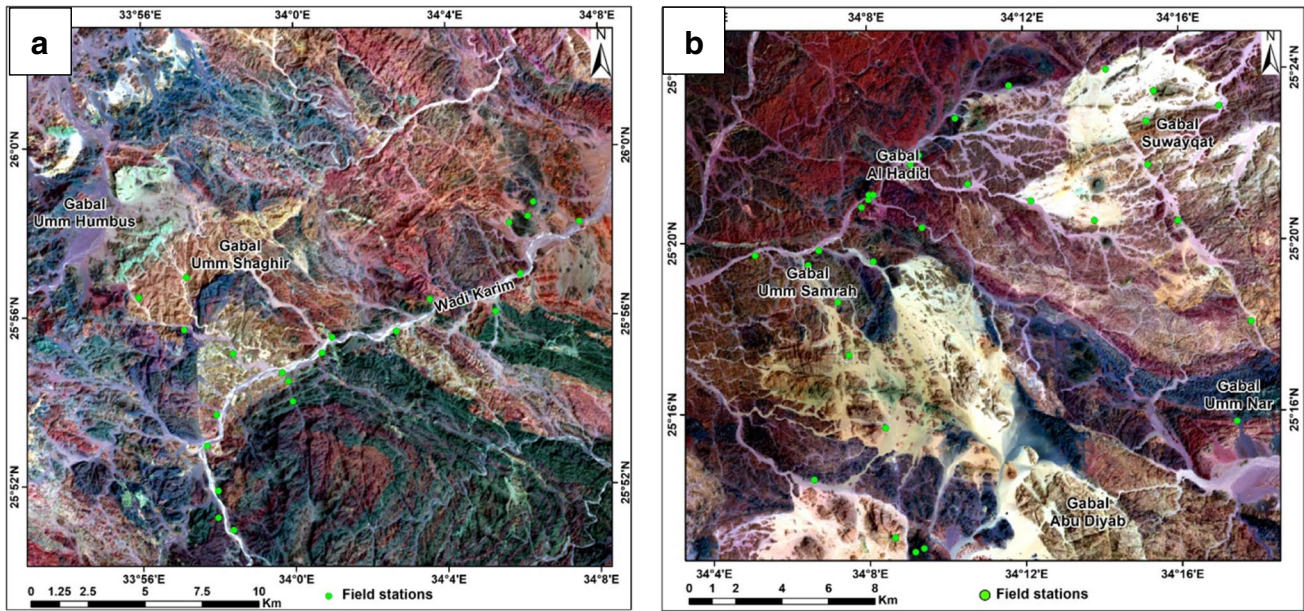
Fig. 5 Location map for the collected samples from **a** Wadi Karim area, **b** Gabal El-Hadid area

Table 1 Eigenvector statistics for selected Landsat-8 bands (2, 4, 5 and 6) for iron minerals of Wadi Karim area

	Band 2	Band 4	Band 5	Band 6
PC 1	0.933527	0.355962	-0.02788	0.032264
PC 2	-0.311288	-0.854834	0.409056	-0.070934
PC 3	0.153506	0.353169	0.894346	0.227711
PC 4	-0.089795	-0.133496	-0.178999	0.970606

The highlighted cells represent the highest iron loads at Wadi Karim area; they are found corresponding to PC1

Table 2 Eigenvector statistics for selected Landsat-8 bands (2, 4, 5 and 6) for iron minerals of Gabal El-Hadid area

	Band 2	Band 4	Band 5	Band 6
PC 1	0.950062	-0.31083	-0.02369	0.014336
PC 2	-0.22942	-0.75125	0.615088	-0.06828
PC 3	0.193911	0.546417	0.769442	0.26793
PC 4	-0.08454	-0.2011	-0.17048	0.960909

The highlighted cells represent the highest iron loads at Gabal El-Hadid area; they are found corresponding to PC2

component analysis was carried out on the selected maximum reflectance and absorption bands of various iron minerals. It is found that for Wadi Karim area, PC1 has high positive loading from bands 2 and 4 with values of 0.933527 and 0.355962, respectively. Thus, iron minerals at Wadi Karim area are illustrated as bright pixels in the principal component band (1); density slicing was carried out on this PC1, and the areas enriched in iron
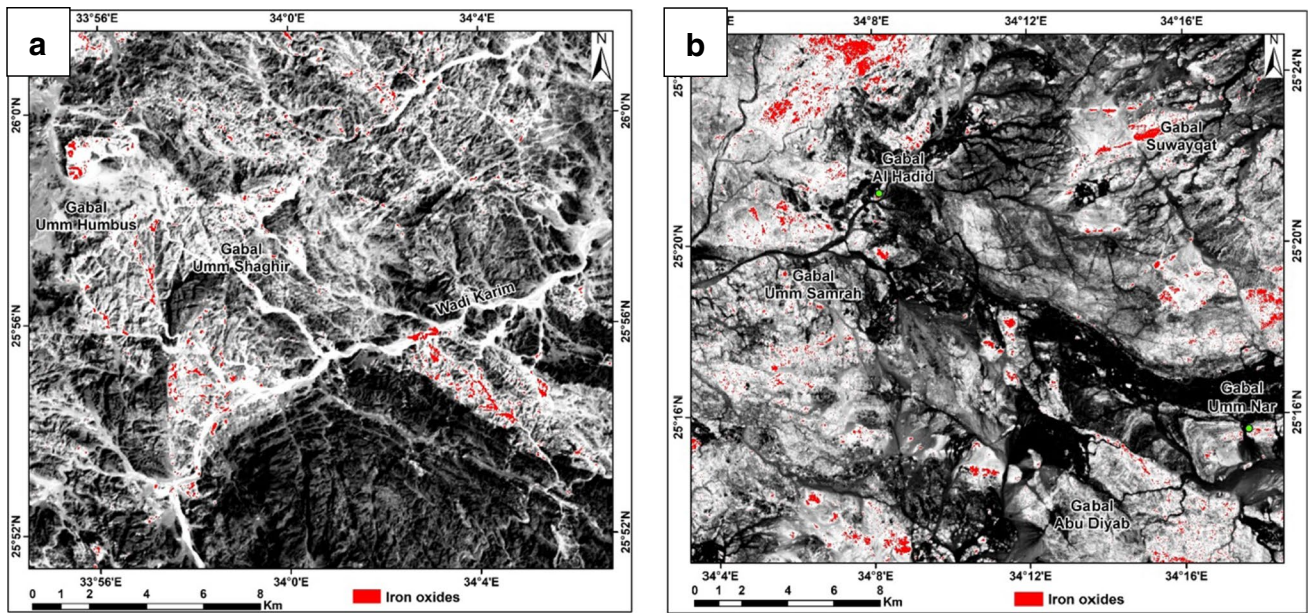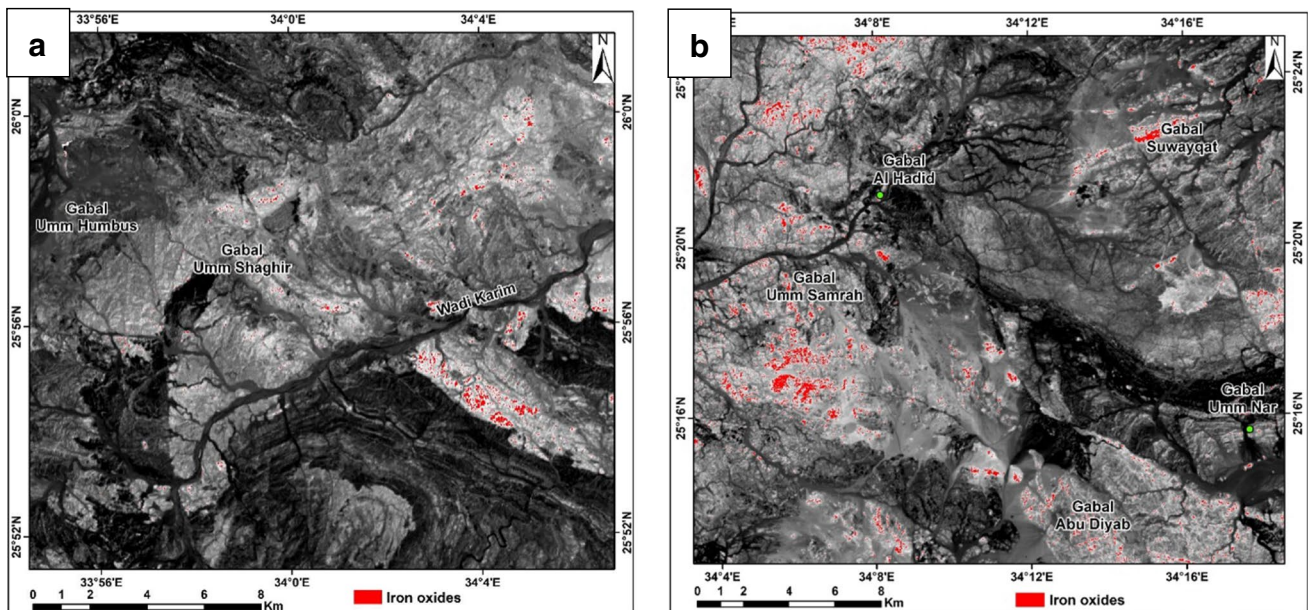
Fig. 6 Iron distribution as yielded from CPCA technique at Wadi Karim area (**a**) and at Gabal El-Hadid area (**b**)

were delineated (Fig. 6a). Moreover, for Gabal El-Hadid area, PC2 has high opposite negative and positive loadings from bands 4 and 5 with values of -0.75125 and 0.615088, respectively. Thus, iron minerals at Gabal El-Hadid area are illustrated as dark pixels in the principal component band (2), density slicing was carried out on this PC2, and the areas enriched in iron were delineated (Fig. 6b).

b. Band ratio technique

The use of band ratio 6/2 was found to be the best and more effective in discriminating the iron-rich rocks for both the studied areas (Fig. 7a and b). This adopted band ratio was selected based on the spectral analyses of the maximum and minimum reflectance values of various iron minerals and their corresponding bands.

Fig. 7 Iron distribution as yielded from the proposed BR technique at Wadi Karim area (**a**) and at Gabal El-Hadid area (**b**)

c. CEM supervised classification using the spectral signatures

The result of CEM supervised classification technique showed the spatial distribution of the iron-rich rocks with signatures similar to those of the input spectra. By the CEM technique, new iron-rich areas having similar spectral signatures as the input USGS iron mineral signatures (Fig. 4) were delineated. The new provided iron-rich localities are highlighted with red colour (Fig. 8a and b).

Interpretation of the field geology and validation of the remote sensing results

The field work validated the newly obtained iron occurrences by the remote sensing techniques at both Wadi Karim and Gabal El-Hadid areas. They are situated in the same geological environments of the existing iron deposits, forming sharply defined stratigraphic units within layered volcanic-volcaniclastic calc-alkaline rocks of andesitic composition.

a. Geology of Wadi Karim iron occurrences

The Wadi Karim main occurrence is located at the intersection of lat. 25° 54′ N and long. 34° 09′ E. BIFs of Wadi Karim area are mainly composed of magnetite and little hematite, goethite as well as limonite and some silica minerals. Quartz, chlorite, biotite and clay minerals are mainly present as gangue minerals. The iron ore is found in the form of ribbons or rows within the pre-Cambrian metamorphic rocks (Fig. 9 a and b). Four layers are intercalated within the host rocks in a sector of 130-m thickness. The most important of these layers is the first layer (the topmost layer) as it extends to more than 3 km along the NW direction, with interface of about 22 m in the direction of the NE slope and thickness ranging from 3.5 to 12 m. These layers are submerged in a series of repetitive convex folds that enclose several small folds. The iron ore in Wadi Karim area is suitable for exploitation as it is more than 1.5 m thick and has large extension, with more than 40% native Fe. The crude reserves are about 17.8 million tons Hussein (1990). The average chemical composition as reported by Hussein (1990) is shown in Table 3.

b. Geology of Gebel El-Hadid occurrence

The iron ore occurrence of Gabal El-Hadid is located at the intersection of lat. 25° 20′ N and long. 34° 34′ E. The iron ore in this occurrence is found in the form of strips and as alternating rows in the metavolcanic

Table 3 Average chemical analysis of Wadi Karim iron, Hussein (1990)

Constituents	Average content, %
Fe	44.0–45.0
SiO_2	23.3–23.5
Ca O + Mg O	8.7
P	0.2–0.3
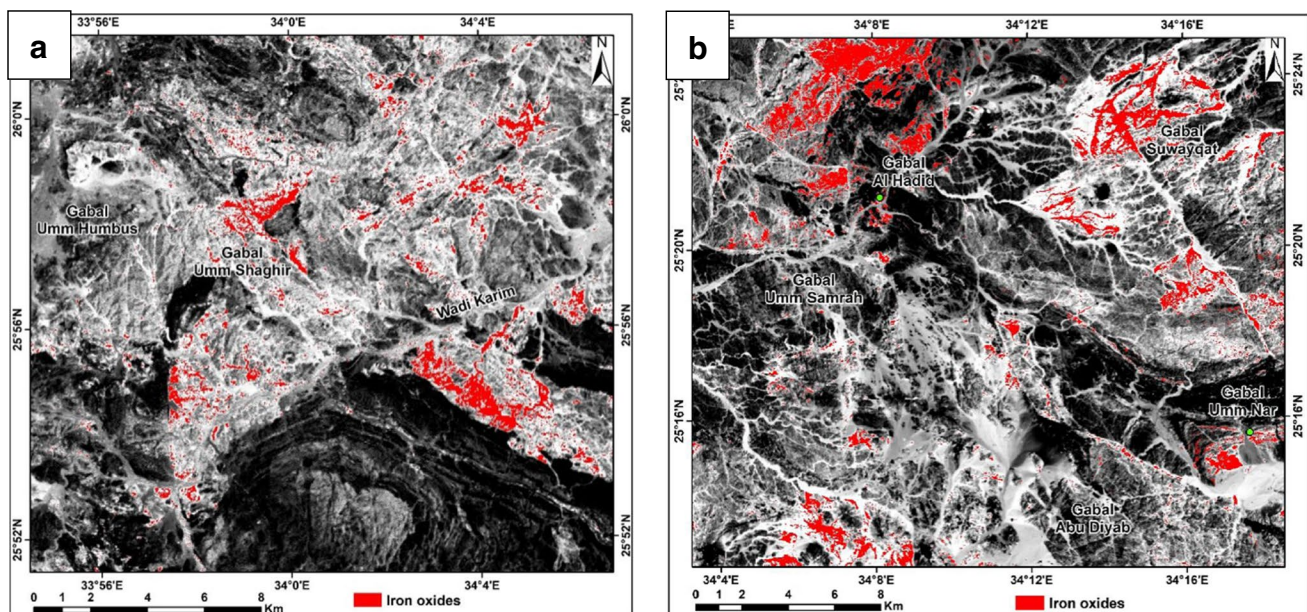
Fig. 8 Iron distribution as yielded from the CEM technique at Wadi Karim area (**a**) and at Gabal El-Hadid area (**b**)

**Table 4** Average chemical composition of Gebel El-Hadid iron ore (after Hussein 1990)

Constituent	Content range %
Fe	43.00–47.00
SiO_2	23.50–25.00
P	0.26–0.29
CaO	2.98–5.40
MgO	0.60
S	0.15–0.40

sequence (Fig. 10 a and b). The BIFs range from few centimetres to more than 10 m in lengths and up to half meter thicknesses, where the iron-rich bands alternate with jasper or sometimes carbonates or silicate bands, frequently faulted and folded with steeply dipping limbs.

Most of the iron forms are present as magnetite, partly altered to martite, concentrated in black bands, alternating with red jasper or with iron-poor grey greenish bands, while hematite is less frequent. Quartz, chlorite, biotite and clay minerals are mainly present as gangues. The area was subjected to folding, and there are many partitions cutting the iron ore strips. The iron ore strips which can be exploited in this site are varying in thickness from 2 to 3 m, exposed in many interfaces with extensions up to 1 km and native Fe contents of about 47% concentration. The iron ore reserves in this region are around 2.15 million tons, up to the level of the ground, and about 1.4 million tons below the surface (Hussein 1990). The chemical analysis of Gebel El-Hadid iron is shown in Table 4 (after Hussein 1990).
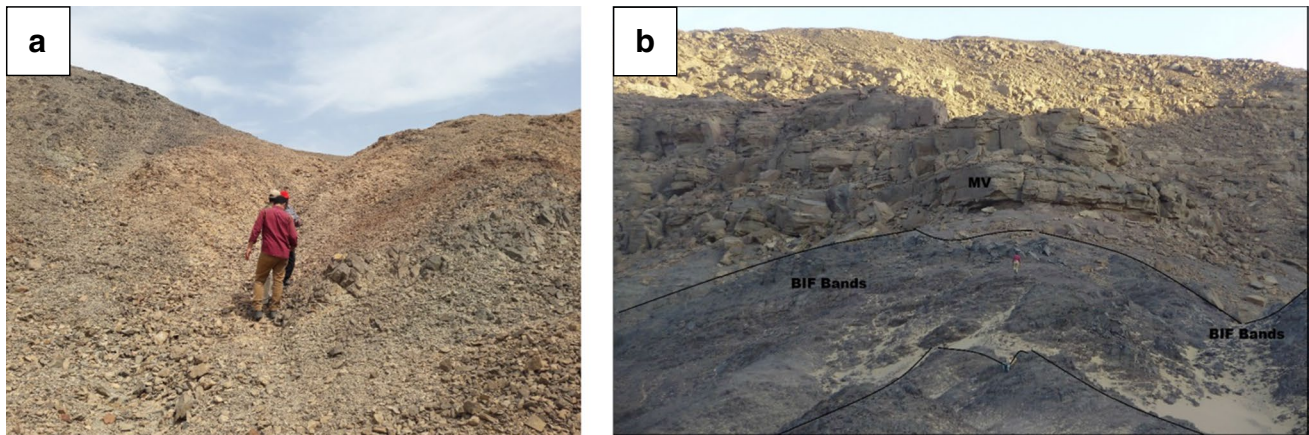
Fig. 9 **a** Iron-rich siltstone of the Hammamat formation in Wadi Karim, looking south; **b** iron-rich siltstone in the detected area, west of Wadi Karim, looking west
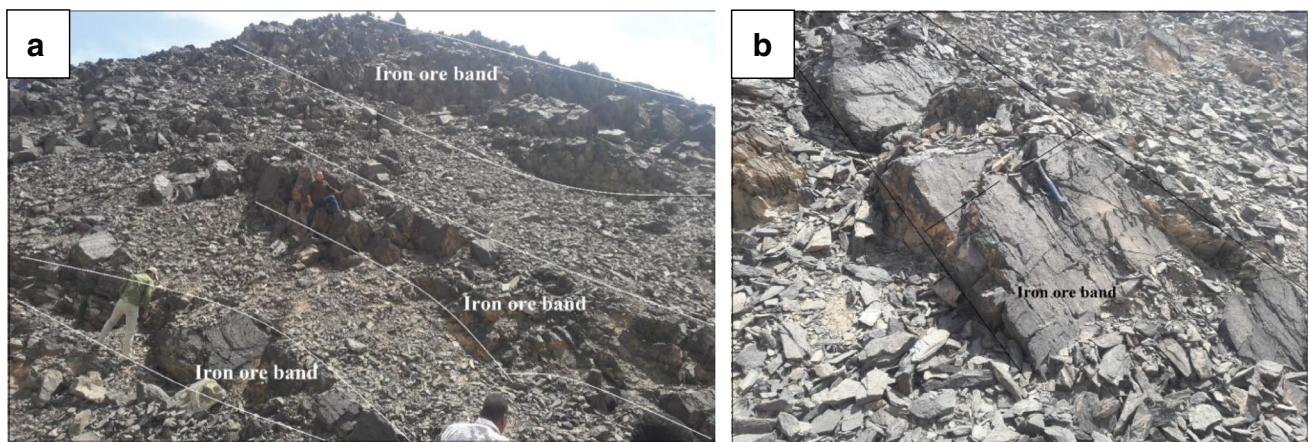
Fig. 10 **a** Iron bands of the existing Gebel El-Hadid area, looking west, and **b** iron bands of the detected area, south east of Gebel El-Hadid, looking east

Discussion

Careful analysis of the spectral signatures of various iron minerals (e.g. hematite, goethite, limonite and magnetite) was the base for band selection especially in the CPCA and the BR techniques, while in the CEM technique, the spectral signatures of these minerals were used as the input in the CEM classifier. Four bands were selected to be analysed using the CPCA technique; two of which represent the maximum reflectance (bands 4 and 6), while the other two represent the maximum absorbance (bands 2 and 5). These four bands were used as the input in the PCA technique, and the result was a four principal component band for each of the studied areas. After analysing the Eigenvector statistics of the results PC bands for Wadi Karim (Table 1) and Gabal El-Hadid (Table 2) areas, it was found that iron distribution in Wadi Karim area is mappable from PC1 and for Gabal El-Hadid area; iron can be delineated from PC2. From the Eigenvector loadings of the PC bands of Wadi Karim area, it is found that the highest loadings are corresponding to PC1, and they have positive values; thus, the iron-rich rocks are illustrated in bright pixels in this PC1 band. Similarly, for Gabal El-Hadid area, the highest loadings were found corresponding to PC2, but they have opposite signs (positive and negative). Because the value with negative sign (-0.75125) is larger than the value with positive sign (0.615088), the iron-rich rocks are illustrated in dark colour on this PC2 band.

The proposed band ratio (B6/B2) was found very effective in discriminating the iron-rich rocks for both the studied areas. The iron-rich rocks were found associated with bright pixels (Fig. 7a and b) The CEM technique was performed through using the spectral signatures of the various iron minerals as reference spectra from the USGS spectral library embedded in the ENVI software. Pixels having similar signatures as the input reference spectra (iron minerals) were mapped as bright pixels. For the adopted three techniques, density slicing was applied to all the results to delineate areas with optimal iron ore occurrence potentiality. Through inspecting all the results, it was observed that the delineated areas by all the techniques came in the same localities. This supports the results. Although the results of all the techniques suggested the same localities for iron potentiality, the result of the proposed band ratio 6/2 technique yielded more concise localities unlike with the other two techniques that resulted in areas with wider distribution. A field study was conducted to the study areas to validate the remote sensing results; samples were collected and field observations were recorded. The field study confirmed and validated the results.

Conclusion

Several satellite image processing techniques were applied on ASTER data and, supported by field work for verification, enabled the delineation of new iron occurrences/ localities guided by the geologic environments of the already existing Wadi Karim and Gabal El-Hadid iron occurrences. The detected iron bands form parallel BIF deposits compatible with the structural planes of the hosting metavolcanics. They are found extending laterally up to almost 3 km; they are observable from several interfaces as dark greyish brown strips of iron with varied thicknesses reaching up to 5 m. The BIFs are composed mainly of magnetite, hematite and silica of jasper, together with a variety of gangue minerals particularly quartz.

The BIF deposits are relatively small mineable reserves distributed in several localities in the study areas. The sporadic distribution of such iron-rich units drives the motivation to carry out more detailed investigations to make the necessary technical and economic feasibility studies and to estimate the exact quality and quantity of these occurrences. In this respect, a local railway line could be constructed connecting each of these localities to transport the iron to the Quseir port.

All in all, the adopted methodology armed with the applied remote sensing techniques showed high efficiency in mapping the iron distribution over the studied areas with extra advantage to the proposed band ratio calculation of B6/ B2 being of relatively higher accuracy. Finally, the applied tools showed high degree of compatibility and efficiency, as the suggested iron areas were proved and validated by the field work.

Declarations

References

Abd El-Wahed MA, Harraz H, El-Behairy MH (2016) Transpressional imbricate thrust zones controlling gold mineralization in the Central Eastern Desert of Egypt. Ore Geol Rev 78:424–446

Abrams MJ, Brown D, Lepley L, Sadowski R (1983) Remote sensing for porphyry copper deposits in southern Arizona. Econ Geol 78(4):591–604

Aiken CL, Balde M, Xu X, Abdel-Salam MG, De La Fuente MF, Mena M (1997) Integrated studies of Mexico with gravity, magnetic, and GIS database. Lead Edge 16(12):1779–1786

Ammar AA, El Sirafe AM, El Kattan EM (1993) Airborne geochemical and structural investigation of the Precambrian copper-bearing rocks, Hammash District, South Eastern Desert Egypt. *Annal Geol Surv Egypt* 19:467–486

Bhattacharya A, Kamaraju MV, Mehta DS, Shrimal AK, Reddy GS (1993) Mathematical modelling for mineral exploration: a case study from Rajpura-Dariba-Lunera mineralized belt, Rajastan India. ITC J 44(4):360–366

Breitkopf JH (1988) Iron formations related to mafic volcanism and ensialic rifting in the southern margin zone of the Damara Orogen Namibia. Precambrian Res 38(2):111–130

Carranza EJM, Hale M (2002) Where porphyry copper deposits are spatially localized? A case study in Benguet province Philippines. Nat Resour J 11(1):45–59

Ciampalini A, Garfagnoli F, Del Ventisette C, Moretti S (2013) Potential use of remote sensing techniques for exploration of iron deposits in Western Sahara and Southwest of Algeria. Nat Resour J 22(3):179–190

Crosta AP, Moore JM (1989) Geological mapping using Landsat thematic mapper imagery in Almeria Province South-east Spain. Int J Remote Sens 10(3):505–514

Crosta AP, De Souza Filho CR, Azevedo F, Brodie C (2003) Targeting key alteration minerals in epithermal deposits in Patagonia, Argentina, using ASTER imagery and principal component analysis. Int J Remote Sens 24(21):4233–4240

Ducart DF, Silva A, Toledo B, Assis L (2016) Mapping iron oxides with Landsat-8/OLI and EO-1/Hyperion imagery from the Serra Norte iron deposits in the Carajás Mineral Province, Brazil. Braz J Geol 46:331–349

Duuring P, Laukamp C (2016) Mapping iron ore alteration patterns in banded iron-formation using hyperspectral data: Beebyn Deposit, Pilbara Craton, Western Australia. Geol Surv West Australia. record 2016/16, p. 18

EGSMA (1997) Geologic map of Al Qusayr Quadrangle and Barrameyia sheets, Egypt. Geol Surv Egypt, Cairo, Egypt

El Habaak GH (2005) Petrogenesis and tectonic implications of the rock succession hosting banded iron formation at Um Anab Area, North Eastern Desert of Egypt. In The Fourth International Conference on the Geology of Africa, Assiut-Egypt (Vol. 2, pp. 479–513)

El-Shazly AK, Khalil KI (2014) Banded iron formations of Um Nar, Eastern Desert of Egypt: P-T–X conditions of metamorphism and tectonic implications. Lithos 196:356–375

Garrels RM (1987) A model for the deposition of the microbanded Precambrian iron formations. Am J Sci 287(2):81–106

Gopinathan P, Parthiban S, Magendran T, Al-Quraishi AMF, Singh AK, Singh PK (2020) Mapping of ferric (Fe^{3+}) and ferrous (Fe^{2+}) iron oxides distribution using band ratio techniques with ASTER data and geochemistry of Kanjamalai and Godumalai, Tamil Nadu, south India. Remote Sens Appl: Soc Environ 18:100306

Gross GA (1980) A classification of iron formations based on depositional environments. Can Mineral 18(2):215–222

Ghoneim SM, Abd El Nabi SH, Yehia MA, Salem SM (2021) Using air-borne gamma ray spectrometry and remote sensing data for detecting alteration zones around wadi Saqia, Central Eastern Desert Egypt. J Afr Earth Sci 178. https://doi.org/10.1016/j.jafrarsci.2021.104181104181

Ghoneim SM, Yehia MA, Salem SM, Ali HF (2022) Integrating remote sensing data, GIS analysis and field studies for mapping alteration zones at Wadi Saqia area, central Eastern Desert Egypt. Egypt J Remote Sens Space Sci 25(1):323–336

Guha A, Saw AK, Mukherjee A, Verma CB, Kumar KV, Rao PVN, Diwakar PG (2020) Eigen vector based analysis of Landsat OLI principal components and constrained energy minimization maps for discriminating iron enriched zones in banded iron formation (BIF) in Sidhi, Madhya Pradesh. Geocarto Int, 37(7):1880–1898

Hamimi Z, Abd El-Wahed MA (2020) Suture(s) and shear zones in the Neoproterozoic basement of Egypt. In Hamimi, Z., El-Baroky, A., Frías, J. M., Fritz, and Abd El-Rahman, Y. (Ed.), The Geology of Egypt. In the ''Regional Geology Reviews'' series, Springer, ISBN: 978–3–030–15264–2, https://doi.org/10.1007/978-3-030–15265–9.

Holland HD (1973) The oceans; a possible source of iron in iron-formations. Econ Geol 68(7):1169–1172

Hussein AA (1990) Mineral deposits. In: Said R (ed) The geology of Egypt. Balkema, Rotterdam, pp 511–566

James BR, Rabenhorst MC, Frigon GA (1992) Phosphorus sorption by peat and sand amended with iron oxides or steel wool. Water Environ Res 64(5):699–705

Kaufman YJ, Sendra C (1988) Algorithm for automatic atmospheric corrections to visible and near-IR satellite imagery. Int J Remote Sens 9(8):1357–1381

Klein C, Beukes NJ (1993) Sedimentology and geochemistry of the glaciogenic late Proterozoic Rapitan iron-formation in Canada. Econ Geol 88(3):542–565

Klein C, Ladeira EA (2004) Geochemistry and mineralogy of Neoproterozoic banded iron-formations and some selected, siliceous manganese formations from the Urucum District, Mato Grosso do Sul Brazil. Econ Geol 99(6):1233–1244

Krapez B, Barley ME, Pickard AL (2003) Hydrothermal and resedimented origins of the precursor sediments to banded iron formation: sedimentological evidence from the Early Palaeoproterozoic Brockman Supersequence of Western Australia. Sedimentology 50(5):979–1011

Lascelles DF (2013) Plate tectonics caused the demise of banded iron formations. Appl Earth Sci 122(4):230–241

Loizenbauer J, Wallbrecher E, Fritz H, Neumayr P, Khudeir AA, Kloetzli U (2001) Structural geology, single zircon ages and fluid inclusion studies of the Meatiq metamorphic core complex: implications for Neoproterozoic tectonics in the Eastern Desert of Egypt. Precambrian Res 110(1–4):357–383

Lottermoser BG, Ashley PM (2000) Geochemistry, petrology and origin of Neoproterozoic ironstones in the eastern part of the Adelaide Geosyncline South Australia. Precambrian Res 101(1):49–67

Loughlin WP (1991) Principal component analysis for alteration mapping. Photogramm Eng Rem S 57(9):1163–1169

Mao Y, Wang D, Liu S, Song L, Wang Y, Zhao Z (2019) Research and verification of a remote sensing BIF model based on

spectral reflectance characteristics. J Indian Soc Remote Sens 47(6):1051–1061

Moradpour H, Rostami Paydar G, Feizizadeh B, Blaschke T, Pour AB, Valizadeh Kamran K, Hossain MS (2022) Fusion of ASTER satellite imagery, geochemical and geology data for gold prospecting in the Astaneh granite intrusive, West Central Iran. Int J Image Data Fusion 13(1):71–94

Moradpour H, Rostami Paydar G, Pour AB, Valizadeh Kamran K, Feizizadeh B, Muslim AM, Hossain MS (2020) Landsat-7 and ASTER remote sensing satellite imagery for identification of iron skarn mineralization in metamorphic regions. Geocarto Int 37(7):1971–1998

Mücke A, Annor A, Neumann U (1996) The Algoma-type iron-formations of the Nigerian metavolcano-sedimentary schist belts. Miner Deposita 31(1):113–122

Pelleter E, Cheilletz A, Gasquet D, Mouttaqi A, Annich M, El Hakour A, Féraud G (2007) Hydrothermal zircons: a tool for ion microprobe U-Pb dating of gold mineralization (Tamlalt–Menhouhou gold deposit—Morocco). Chem Geol 245(3–4):135–161

Ramadan TM, Kontny A (2004) Mineralogical and structural characterization of alteration zones detected by orbital remote sensing at Shalatein District, SE Desert Egypt. J Afr Earth Sci 40(1–2):89–99

Ruiz-Armenta JR, Prol-Ledesma RM (1998) Techniques for enhancing the spectral response of hydrothermal alteration minerals in thematic mapper images of Central Mexico. Int J Remote Sens 19(10):1981–2000

Sabins FF (1997) Remote sensing principles and interpretation. W. H. Freeman Company, New York, pp 366–371

Sadiya TB, Ibrahim O, Asma TF, Mamfe V, Nsofor CJ, Oyewmi AS, Ozigis MS (2014) Mineral detection and mapping using band ratioing and Crosta technique in Bwari Area Council, Abuja Nigeria. Int J Sci Eng Res 5(12):1100–1108

Salem SM, El Gammal EA (2015) Iron ore prospection East Aswan, Egypt, using remote sensing techniques. Egypt J Remote Sens Space Sci 18(2):195–206

Salem SM, El Gammal EA, Soliman NM (2013) Morphostructural record of iron deposits in paleosols, cretaceous Nubia Sandstone of Lake Naser basin, Egypt, Western Desert Egypt. Egypt J Remote Sens Space Sci 16(1):71–82

Sekandari M, Masoumi I, Pour AB, Muslim AM, Hossain MS, Misra A (2022) ASTER and WorldView-3 satellite data for mapping lithology and alteration minerals associated with Pb-Zn mineralization. Geocarto Int 37(6):1782–1812

Tangestani MH, Moore F (2001) Comparison of three principal component analysis techniques to porphyry copper alteration mapping: a case study, Meiduk area, Kerman Iran. Can J Remote Sens 27(2):176–182

Tangestani MH, Moore F (2002) Porphyry copper alteration mapping at the Meiduk area Iran. Int J Remote Sens 23(22):4815–4825

Traore M, Çan T, Tekin S (2020) Discrimination of iron deposits using feature oriented principal component selection and band ratio methods: Eastern Taurus/TURKEY. Int J Environ Geoinform 7:147–156

Trendall AF, Blockley JG (2004) Precambrian iron-formation The Precambrian earth: tempos and events. Elsevier, Amsterdam, pp 403–421